Russian Chemical Reviews **82** (3) 273 – 288 (2013) © 2013 Russian Academy of Sciences and Turpion Ltd

DOI 10.1070/RC2013v082n03ABEH004343

High-temperature oxidation of copper

V V Belousov, A A Klimashin

Contents

I. Introduction 273
II. Kinetics of high-temperature oxidation of copper 273
III. Kinetics and mechanism of catastrophic oxidation of copper 278

Abstract. Data on the kinetics and thermodynamics of high-temperature oxidation of copper are generalized. The attention is focused on the catastrophic oxidation of copper contacting some low-melting oxides. The results of experimental and theoretical studies of the last 10 years concerning the catastrophic oxidation of copper are analyzed. The theory of catastrophic oxidation of copper under a thin layer of low-melting oxide is considered. The bibliography includes 135 references.

I. Introduction

Copper finds wide use as a thermal conductor in cooling devices used in space engineering, metallurgy, fuel and nuclear engineering, *etc*.[1] In these devices, copper is often in contact with refractory metals and their alloys. However, not all of refractory metals in contact with copper ensure sufficient safety margin of cooling devices under oxidizing atmosphere. For instance, catastrophic (accelerated) copper oxidation can occur in the systems Cu – Mo, Cu – W and Cu – V due to formation of low-melting oxides of refractory metals.[2, 3] The enhancement of the safety margins of cooling devices is largely dependent on the development of views about the mechanism of catastrophic oxidation of copper.

A considerable contribution to the understanding of the mechanism of high-temperature oxidation of copper was made by Wagner.[4] The theory of Wagner was repeatedly confirmed in experiments, but only for dense and solid oxide layers formed on the copper surface in the course of high-temperature oxidation. However, during catastrophic oxidation when a dense oxide layer containing a liquid phase is formed on the surface, the oxidation rate substantially increases and exceeds the oxidation rate implied by the Wagner model by orders of magnitude.[5]

The problem of accelerated oxidation of metals and alloys is under active discussion.[6 – 51] Recently, significant progress in understanding of the catastrophic oxidation of copper has been made. Two stages, *viz*., fast and super-fast ones, were detected in this process.[52]

The high-temperature oxidation of copper is adequately covered in the book of Kofstad.[53] A review by Belousov [54] is devoted to the catastrophic oxidation of copper. The present review differs by that a single approach is used to consider both high-temperature oxidation of copper, to which the classic model of Wagner is applicable, and catastrophic oxidation for which new models have been developed.[55 – 57] The experimental and theoretical results obtained in this field for the past ten years are also discussed.

II. Kinetics of high-temperature oxidation of copper

The mechanism of high-temperature oxidation of copper was the subject of numerous experimental and theoretical studies of the first and beginning of the second half of the last century.[58 – 68] It was established that in the temperature range of 350 – 1050 °C, copper is oxidized according to a parabolic time law. The temperature dependences of the parabolic rate constants (k'') obtained by different authors are shown in Fig. 1, the derived activation energy values for this process are presented in Table 1. Three regions can be distinguished in the temperature dependence, *viz*., high-temperature (900 – 1050 °C), intermediate (600 – 850 °C) and low-temperature (350 – 550 °C) regions.

In the opinion of Mrowec and Stoclosa,[69] the discrepancy of the temperature dependences of the copper oxidation rates obtained by different authors is due to errors in determination of the rate constant. Commonly, rate constants were derived without taking into account the changes in the copper surface area in the course of oxidation. However, this opinion is not sufficiently convincing because high-temperature oxidation studies are performed most often using 0.1 – 0.5 mm thick metallic plates, and the area of such plates changes insignificantly during the experi-

V V Belousov, A A Klimashin A A Baikov Institute of Metallurgy and Materials Science, Russian Academy of Sciences, Leninsky prosp. 49, 119991 Moscow, Russian Federation. Tel. (7-495) 718 16 55, e-mail: vbelousov@imet.ac.ru (V V Belousov), klim@imet.ac.ru (A A Klimashin)

Received 13 July 2012
Uspekhi Khimii **82** (3) 273 – 288 (2013); translated by S E Boganov

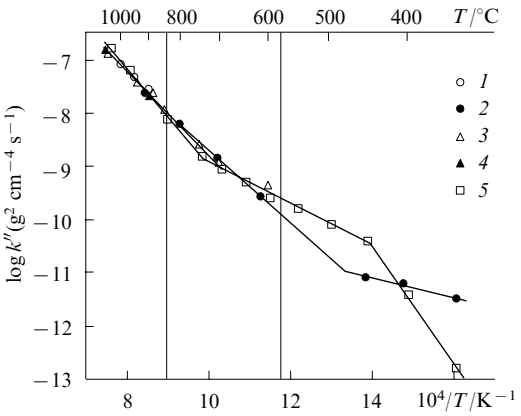


Figure 1. Temperature dependences of the parabolic rate constant for oxidation of copper from Refs 69 (*1*), 70 (*2*), 71 (*3*), 72 (*4*) and 73 (*5*).

ment.[77,78] However, kinetic studies of the oxidation of nickel,[79] zinc,[80] cobalt,[81] zirconium and hafnium[82] have showed that the rate constant of the process depends on the material purity.

To elucidate the sources of the above-mentioned discrepancies, Zhu *et al.*[83] studied the mechanism of oxidation of copper depending on its purity in the temperature range of 350–1050 °C. The study was performed with three types of copper samples shaped like 0.4–0.5 mm-thick discs with a diameter of 5 mm, namely

— copper purified by zone melting (ZMP copper) of >99.9999% purity,

— copper 6N of 99.9999% purity,

— copper 6N of 99.99% purity.

The content of impurities in these samples is given in Table 2. Before oxidation, the samples were heated at 600 °C for 24 h under a hydrogen atmosphere. The changes in their area during oxidation were calculated by the formula proposed by Mrowec and Stoclosa.[69] The change in the rate constants turned out to be insignificant.

Table 1. Activation energy (E_a) of the high-temperature oxidation of copper.

Purity (%)	Atmosphere	T/°C	E_a/kJ mol^{-1}	Ref.
99.999	air	900–1050	140	69
99.99	"	300–500	39	70
99.99	"	600–900	123	70
99.99	oxygen	700–1000	132	71
99.995	air	900–1050	159	72
99.999	oxygen or air	750–1040	172	73
99.999	the same	450–750	84	73
9.999	"	350–450	223	73
99.9	air	750–1000	146	74
99.999	oxygen	660–937	179	75
99.99	"	300–550	84	76
99.99	"	550–900	158	76

The kinetics of oxidation of copper of different purity in the range of 350–1050 °C is presented in the parabolic coordinates in Fig. 2. The linear nature of these dependences indicates that the copper oxidation proceeds in the diffusion mode. In the temperature range of 900–1050 °C, all the samples are oxidized at nearly the same rate. Upon lowering the temperature to 600 °C, the oxidation rate depends on the purity of copper and increases in the following series:

$$\text{ZMP} \leqslant \text{6N} < \text{4N}$$

At temperatures of <600 °C, the 4N sample is oxidized slower than the ZMP and 6N samples, which are oxidized at virtually the same rates.

Table 2. Concentrations of impurities in the copper samples (10^{-4} mass %).[83–86]

Impurity	Copper sample		
	ZMP	6N	4N
Al	—	0.4	1.1
Si	0.004	0.3	1.5
P	—	0.01	4.2
S	0.003	0.06	4.1
Fe	—		0.7
Ni	—	0.004	0.4
Se	—	0.3	0.2
As	0.003	0.01	0.4
Sb	—		0.9
Ag	—	0.008	5.5
Bi	—		0.06
Pb	—	0.04	

The temperature dependences of parabolic rate constants for oxidation of copper of different purity are shown in Fig. 3. Note that there are three regions in these curves, as in similar curves shown in Fig. 1: high-temperature (900–1050 °C), intermediate (600–850 °C) and low-temperature (350–550 °C) regions. The derived activation energies in the high-temperature region are almost the same for all samples and are equal to ~173 kJ mol^{-1}. For the intermediate and low-temperature regions, the values of E_a (kJ mol^{-1}) are the following:

Sample	ZMP	6N	4N
$E_{a\ (600-800\ °C)}$	93	111	95
$E_{a\ (350-550\ °C)}$	40	40	52

Smeltzer *et al.*[84] demonstrated that copper oxidation in the temperature range of 600–1050 °C results in predominant growth of the Cu_2O phase; the rate-determining step of the process is bulk diffusion of copper cations in the crystal lattice of Cu_2O. It was noted that in the intermediate temperature region, grain-boundary diffusion is also possible along with bulk diffusion. The mechanism of copper oxidation in the temperature range of 350–500 °C was also studied.[70,73,76] It was established that the rate of copper oxidation is controlled by grain-boundary diffusion in this temperature range.

Typical microstructures of oxide layers on the surface of ZMP copper pre-oxidized at 1000, 800, 600 and 400 °C are shown in Fig. 4. The temperature dependences of the volume fraction of CuO in the oxide layers of ZMP, 6N and 4N copper samples are depicted in Fig. 5.

The effect of grain-boundary diffusion on the kinetics of copper oxidation was estimated.[84] The oxidation rate can be expressed as follows:

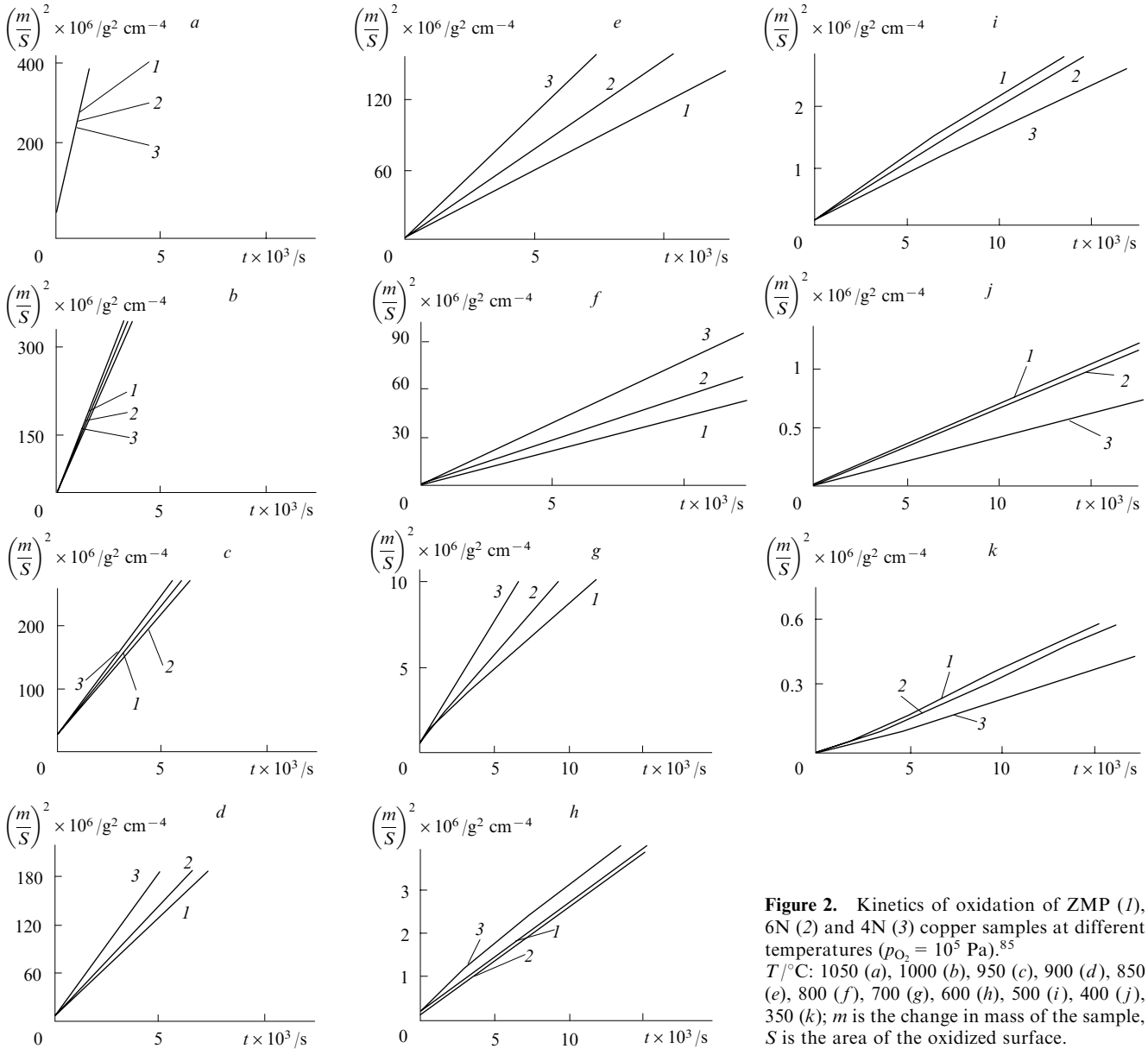


Figure 2. Kinetics of oxidation of ZMP (*1*), 6N (*2*) and 4N (*3*) copper samples at different temperatures ($p_{O_2} = 10^5$ Pa).[85]
T/°C: 1050 (*a*), 1000 (*b*), 950 (*c*), 900 (*d*), 850 (*e*), 800 (*f*), 700 (*g*), 600 (*h*), 500 (*i*), 400 (*j*), 350 (*k*); m is the change in mass of the sample, S is the area of the oxidized surface.

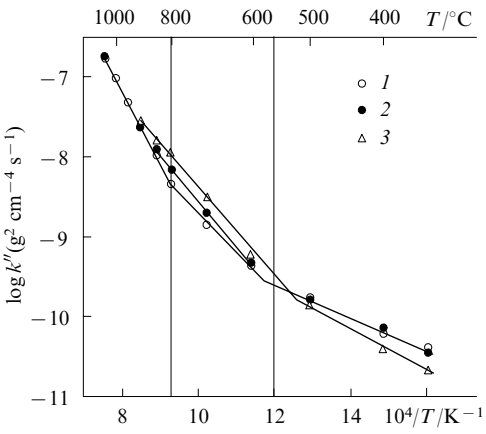


Figure 3. Temperature dependences for the parabolic rate constant of oxidation of copper of different purity ($p_{O_2} = 10^5$ Pa). Copper samples: ZMP (*1*), 6N (*2*) and 4N (*3*).[86]

$$\frac{d(x^2)}{dt} = 2D_v V \Delta c + \frac{4D_b V \Delta c \delta}{d_t} \quad (1)$$

where x is thickness of the oxide layer at time t; D_v is the bulk diffusion coefficient; V is the molar volume of the oxide; Δc is the concentration gradient of point defects in Cu_2O (across the oxide layer); D_b is the grain-boundary diffusion coefficient; δ is the width of grain boundaries; d_t is a mean size of grains at time t.

Equation (1) is nothing but

$$\frac{d(x^2)}{dt} = k''_\Sigma = k''_v + k''_b f \quad (2)$$

where k''_Σ is the overall parabolic rate constant; k''_v is a term related to bulk diffusion in the lattice; k''_b is the term due to grain-boundary diffusion; $f = 2\delta/d_t$ is the fraction of all diffusion areas located at grain boundaries.

Therefore, the contribution from the grain-boundary diffusion can be estimated by the formula

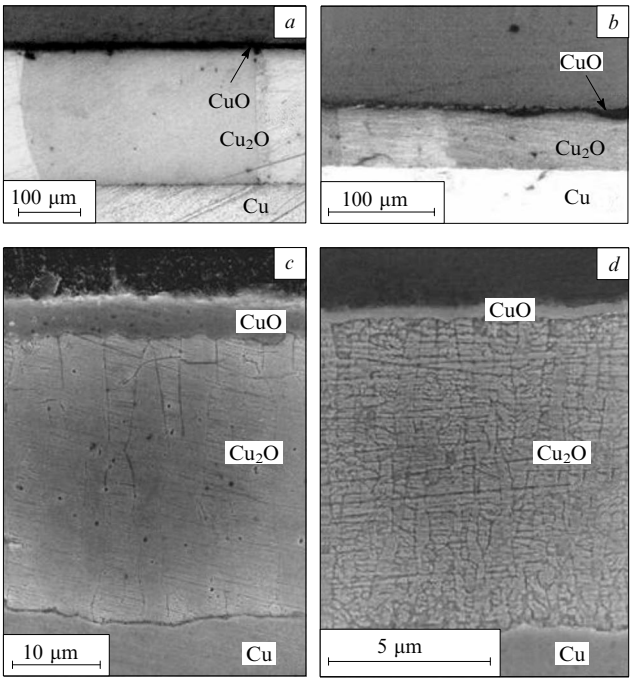


Figure 4. Micrographs of oxide layers on ZMP copper oxidized under oxygen atmosphere ($p_{O2} = 10^5$ Pa) for 30 min at 1000 °C (*a*), for 30 min at 800 °C (*b*), for 240 min at 600 °C (*c*), for 480 min at 400 °C (*d*).[86]

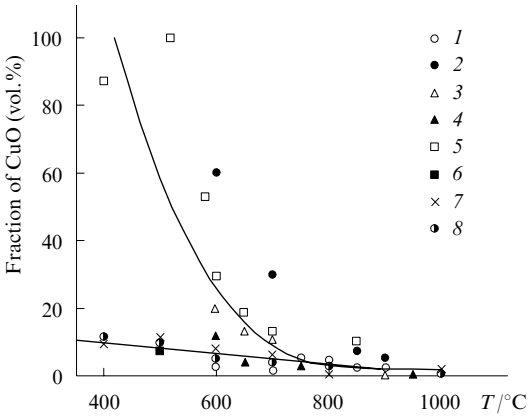


Figure 5. Temperature dependences of the CuO volume fraction in the oxide layer ($p_{O_2} = 10^5$ Pa) according to Refs 71 (*1*), 81 (*2*), 87 (*3*), 88 (*4*), 70 (*5*), 86 (*6–8*).
(*6–8*) are for samples of ZMP, 6N, 4N copper, respectively.

$$\frac{k''_b f}{k''_v} = \frac{2D_b\delta}{D_v d_t} \qquad (3)$$

which implies that establishing the degree of influence of the grain-boundary diffusion on the kinetics of copper oxidation requires considering the density of boundaries of Cu_2O grains in the oxide layer. The larger the average size of Cu_2O grains, the lower the density of grain boundaries in the oxide layer, and the lower the contribution from grain-boundary diffusion, and *vice versa*. Columnar grains of Cu_2O are rather large in ZMP copper oxidized at 800 and 1000 °C (see Fig. 4 *a*,*b*); however, their average size is

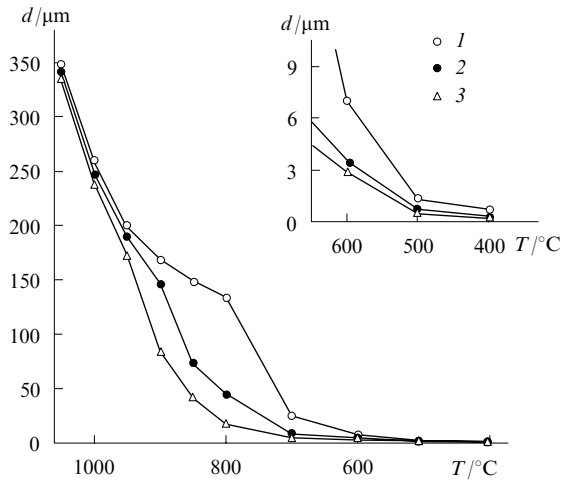


Figure 6. Temperature dependences of the average size of Cu_2O grains in the oxide layer formed after oxidation ($p_{O_2} = 10^5$ Pa) of the ZMP (*1*), 6N (*2*) and 4N (*3*) copper samples.[83]

smaller if copper is oxidized in the temperature range of 400–600 °C. The temperature dependences of the average size of Cu_2O grains in the oxide layers formed upon oxidation of ZMP, 6N and 4N copper samples are shown in Fig. 6. The average size of Cu_2O grains is $\sim$100 μm for the high-temperature region and <1 μm for the intermediate and low-temperature regions.

Therefore, bulk diffusion prevails in the high-temperature region due to formation of larger grains of Cu_2O in the oxide layer. In the intermediate region, bulk and grain-boundary diffusions operate simultaneously. Presumably, the decrease in activation energy in the intermediate temperature range is related to the contribution of grain-boundary diffusion. Grain-boundary diffusion is prevalent in the low-temperature region. As the temperature decreases, the contribution from grain-boundary diffusion increases, and the activation energy of the process decreases. Thus, bulk diffusion makes a significant contribution to the oxidation of copper at high temperatures, whereas grain-boundary diffusion plays an important role at temperatures below 0.4 $T_{m\,Cu}$.

In the high-temperature region where bulk diffusion is predominant (see Figs 1 and 3), the oxidation rates for copper samples of different purity are practically the same. This indicates that impurities have little effect on the kinetics of copper oxidation. Nevertheless, in intermediate- and low-temperature regions, the oxidation rates depend on the content of impurities in copper. It is possible that the lower rates of oxidation and higher activation energies for less pure copper in the low-temperature region may be related to the segregation of impurities at the Cu_2O grain boundaries, which restricts the rate of diffusion.[89, 90]

The kinetics of copper oxidation depending on temperature and oxygen partial pressure is presented in Fig. 7 and 8, respectively. The oxidation rate increases with increasing temperature and partial pressure of oxygen. Plots (*1–5*) in Fig. 8 correspond to the partial pressure of oxygen at which CuO is unstable, while plot (*6*) is obtained under partial pressure at which CuO is stable. The double Cu_2O/CuO layer is formed on the copper surface in the latter case.

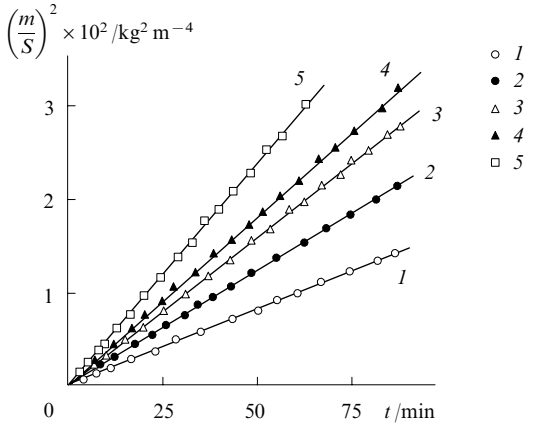


Figure 7. Kinetics of oxidation of copper ($p_{O_2} = 2.6 \times 10^3$ Pa) at 900 (*1*), 950 (*2*), 980 (*3*), 1000 (*4*), 1050°C (*5*).[85]

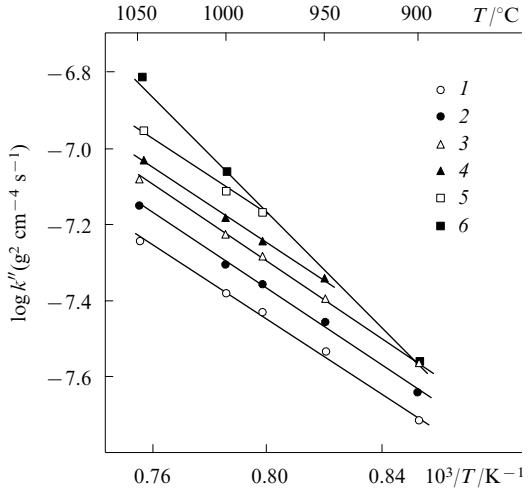


Figure 8. Temperature dependences of the parabolic rate constant for oxidation of copper at oxygen partial pressures of 6.6×10^2 (*1*), 1.3×10^3 (*2*), 2.6×10^3 (*3*), 3.9×10^3 (*4*), 7.9×10^3 (*5*), 2.1×10^4 Pa (*6*).[86]

The dependences of parabolic rate constants for oxidation of copper on the partial pressure of oxygen at different temperatures are shown in Fig. 9. The rate of copper oxidation increases with the oxygen partial pressure up to a certain value. Further increase in p_{O_2} does not result in the increase in the oxidation rate. In region *I* where the oxygen partial pressure is lower than the equilibrium pressure for CuO dissociation, the oxide layer consisting of only Cu_2O is formed. It is known that Cu_2O is a p type semiconductor with deficiency of the metal in which cation vacancies and electron holes are formed.[91–97] The concentration gradient of cation vacancies in Cu_2O increases with oxygen partial pressure. The copper oxidation rate also increases. The formation of defects in Cu_2O is described by the following equation [77]

$$0.5\,O_2 = O_O + 2\,V'_{Cu} + 2\,h^{\bullet} \qquad (4)$$

where V'_{Cu} is the cation vacancy, $h^{\bullet}$ is the electron hole. However, the vacancies and electron holes may combine

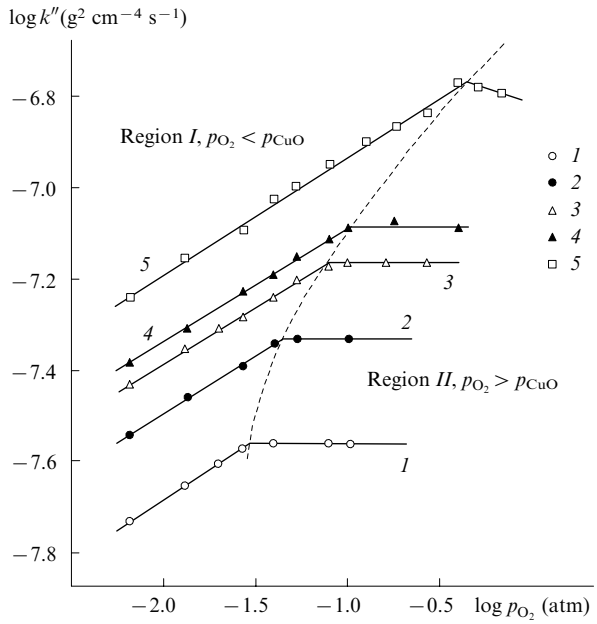


Figure 9. Parabolic rate constants for oxidation of copper *vs.* the oxygen partial pressure at temperatures of 900 (*1*), 950 (*2*), 980 (*3*), 1000 (*4*), 1050 °C (*5*).[77]
The dashed line shows the transition from single-phase oxide layer (region *I*) to two-phase one (region *II*).

forming neutral copper vacancies (V_{Cu}) according to the equation

$$V'_{Cu} + h^{\bullet} = V_{Cu} \qquad (5)$$

The formation of neutral copper vacancies can be expressed by combining equations (4) and (5)

$$0.5\,O_2 = O_O + 2\,V_{Cu} \qquad (6)$$

If formation of the Cu_2O defect structure is described by Eqn (4), then the dependence of the parabolic rate constant for oxidation of copper on the oxygen partial pressure has the form

$$k' \sim (p''_{O_2})^{1/8} \qquad (7)$$

If the Cu_2O defect structure is formed according to Eqn (6), the dependence is as follows:[77]

$$k' \sim (p''_{O_2})^{1/4} \qquad (8)$$

According to dependences shown in Fig. 9, the exponent is very close to 1/4, therefore the neutral cation vacancies should be the major defects in Cu_2O.

In region *II* (see Fig. 9) where the oxygen partial pressure is higher than the CuO dissociation pressure, CuO is formed on the external surface of the Cu_2O layer. The partial pressure of oxygen at the Cu_2O/CuO interface (which determines the concentration gradient of cation vacancies in Cu_2O) does not change and corresponds to the CuO dissociation pressure. Therefore, the rate of oxidation of copper does not depend on the external pressure of oxygen. The mechanism of oxidation of Cu_2O to CuO has been described in detail.[98]

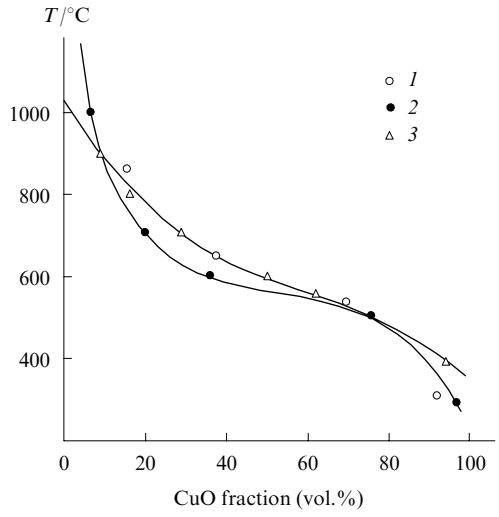


Figure 10. Temperature dependences of the CuO volume fraction in the oxide layer.
(*1*, *2*) Represent experimental and theoretical data of Valensi,[76] respectively, (*3*) Garnaud's calculations by formula (9).[99]

A relation for calculating the ratio of thicknesses of the Cu_2O and CuO layers formed upon high-temperature copper oxidation was derived by Garnaud[99] based on the theory of formation of double oxide layers developed by Yurek *et al.*[100]

$$\frac{L_{CuO}}{L_{Cu_2O}} = -\frac{1}{2}\left(\frac{1}{1.92} - \frac{1.92A}{2}\right) + \frac{1}{2}\sqrt{\left(\frac{1}{1.92} - \frac{1.92A}{2}\right)^2 + 4A} \quad (9)$$

where L_{CuO} is the CuO layer thickness, L_{Cu_2O} is the Cu_2O layer thickness,

$$A = 3.192 \times 10^{-5} \exp\left(\frac{8780}{T}\right) \quad (10)$$

Taking into account Eqn (10), relation (9) indicates that the ratio of oxide layer thicknesses is a function of temperature. The calculated ratios of thicknesses of oxide layers on copper (Fig. 10) agree with the experimental data obtained by Valensi.[76]

It should also be noted that the experimental results of the studies[76, 87] devoted to measurement of the rate of formation of Cu_2O layer on copper correspond to the results of another work.[69] According to the latter work, the A value in Eqn (9) is 0.058 at 900 °C, which corresponds to a 9.2% volume fraction of CuO in the oxide layer. This value almost coincides with the result (9.5%) obtained by Valensi.[76]

III. Kinetics and mechanism of catastrophic oxidation of copper

The term 'catastrophic oxidation' introduced by Leslie and Fontana[101] means accelerated oxidation of metals and alloys contacting with some low-melting oxides at elevated temperatures. For the first time, catastrophic oxidation of copper in contact with MoO_3 at 480 °C in air was described by Rathenau and Meijering.[102] They suggested that the catastrophic oxidation of copper in contact with MoO_3 is related to the formation of liquid phase in the oxide layer. Later, this concept was developed by Belousov.[2, 3, 5, 30, 52, 54–57, 103–106] Two stages, fast and super-fast ones, were revealed in the catastrophic oxidation of copper in contact with Bi_2O_3.[52, 54, 55]

1. Catastrophic oxidation of copper in contact with low-melting oxides Bi_2O_3, MoO_3 and V_2O_5

a. The $Cu-Bi_2O_3$ system

The fast stage of catastrophic oxidation of copper

It was found that copper coated by a thin (10–100 μm) bismuth film is catastrophically oxidized in air at 770 °C (Fig. 11).[2, 5, 52, 55] The rate of oxidation of copper does not depend on the initial form of bismuth (metal, oxide or bismuth cuprate) (Fig. 12), it is affected by the amount of bismuth per unit area of copper.

The dependences of the rates of catastrophic copper oxidation on the Bi_2O_3 film thickness in parabolic coordinates are shown in Fig. 13. The catastrophic oxidation of copper is described by the following law:

$$\left(\frac{m}{S}\right)^2 = k''t \quad (11)$$

where m is the change in mass of the sample, S is the copper surface area, k'' is the parabolic rate constant for oxidation of copper, t is time. This indicates a diffusion-controlled process. The k'' value depends on the thickness of the film

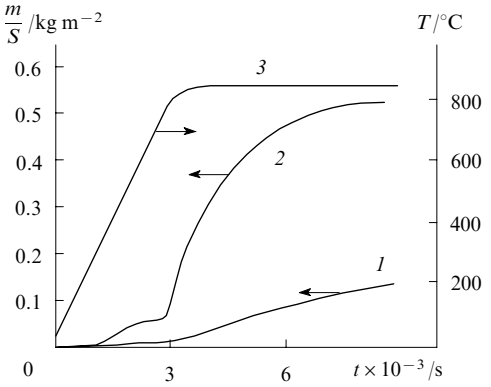


Figure 11. Kinetics of oxidation of copper without a coating (*1*) and with a bismuth film coating (*2*), and temperature change (*3*).[3]

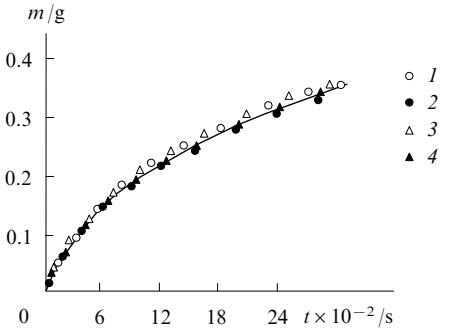


Figure 12. Kinetics of catastrophic oxidation of copper with various coatings at 800 °C.[3]
The coatings are Bi (*1*), Bi_2CuO_4 (*2*), Bi_2O_3 (*3*), $Bi_2CuO_4 + Bi_2O_3$ (*4*); the amount of bismuth per unit area was the same in all cases.

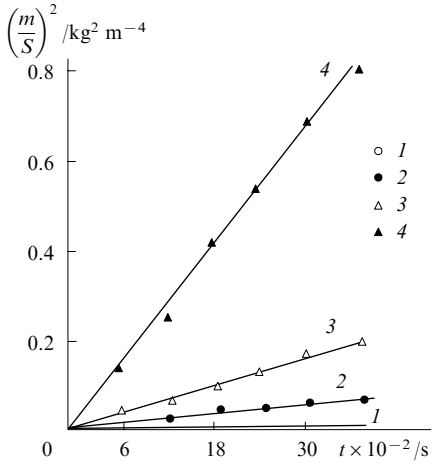


Figure 13. Kinetics of catastrophic oxidation of copper coated by the Bi_2O_3 layer of various thicknesses at 800 °C.[3]
The thicknesses of the coating /10^{-5} m: 0 (*1*), 3 (*2*), 6 (*3*), 9 (*4*); $k''/10^{-5}$ kg^2 m^{-4} s^{-1}: 0.12 (*1*), 1.6 (*2*), 4.9 (*3*), 21 (*4*).

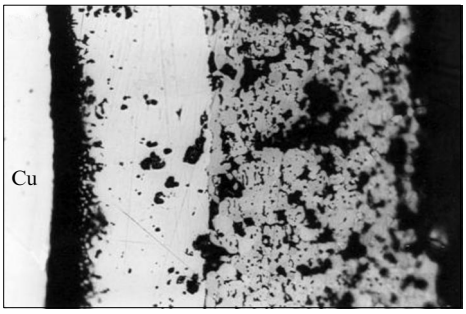


Figure 14. Micrograph of the oxide layer formed after catastrophic oxidation of copper in contact with Bi_2O_3 in air at 800 °C.[3]

and exceeds the parabolic rate constant for oxidation of copper without a film by more than two orders of magnitude.

A micrograph of the double oxide layer formed upon catastrophic oxidation of copper in contact with Bi_2O_3 is shown in Fig. 14. The outer dark part of the oxide layer consists mainly of Bi_2CuO_4. The inner light part is predominantly CuO and some amounts of Cu_2O, Bi_2O_3 and Bi_2CuO_4.

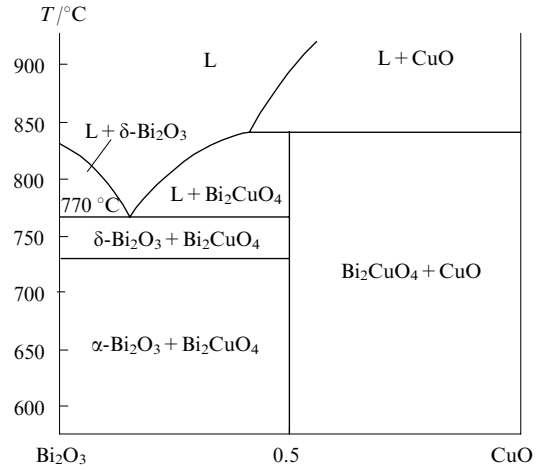


Figure 15. Phase diagram for the Bi_2O_3–CuO system.[107]

In accordance with the Bi_2O_3–CuO phase diagram (Fig. 15), the threshold temperature (770 °C) for catastrophic oxidation of copper in contact with Bi_2O_3 coincides with the eutectic point. Therefore, the catastrophic copper oxidation is related to the formation of the liquid phase in the oxide layer. To reveal the role of this phase, ionic conductivity of model Bi_2CuO_4–Bi_2O_3 composites with respect to oxygen was measured[108–111] above the eutectic point (770°C).

Transport properties of model Bi_2CuO_4–n Bi_2O_3 composites (n = 5 mass %, 10 mass %, 15 mass %, 20 mass %)

It was found[108] that triple grain junctions and grain boundaries are wetted by eutectic melt in Bi_2CuO_4–n Bi_2O_3 composite ceramics (n = 5 mass %, 10 mass %, 15 mass %, 20 mass %) at 770 °C. Consider this phenomenon taking Bi_2CuO_4–20 mass % Bi_2O_3 composite ceramics as an example. In the starting microstructure of this composite, the light Bi_2O_3 phase is randomly distributed in the composite bulk (Fig. 16 *a*). As the composite is heated above 770 °C, the triple grain junctions and some grain boundaries are wetted by the eutectic melt and a liquid-channel grain-boundary structure is formed (Fig. 16 *b*,*c*). The microstructure of the quenched wetting melt at triple grain-boundary junctions is shown in Fig. 17. The micrograph confirms the existence of the eutectics. The formation of the liquid-

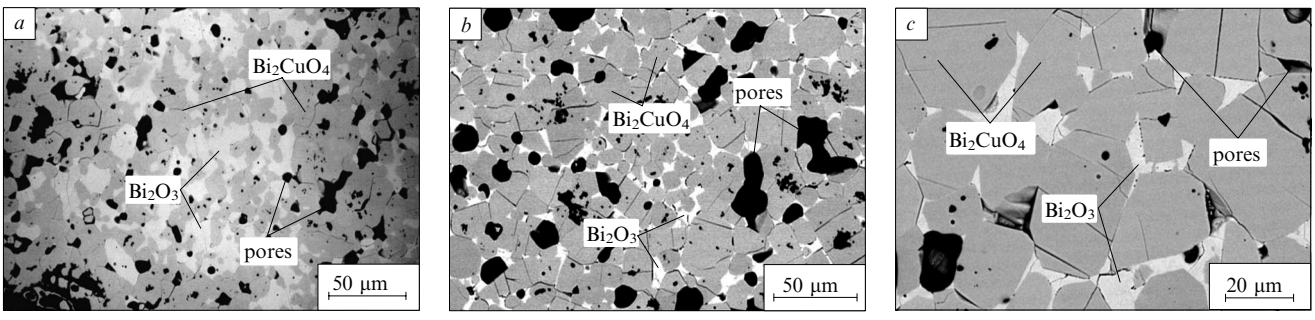


Figure 16. Micrographs of the Bi_2CuO_4–20 mass % Bi_2O_3 ceramic composite.[108]
(*a*) Cooling from 700 °C; (*b*, *c*) cooling from 780 °C.

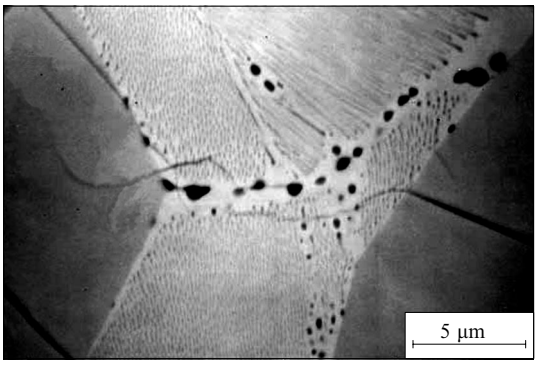


Figure 17. Micrograph of the solidified wetting melt at a triple Bi_2CuO_4 grain junction.[108]

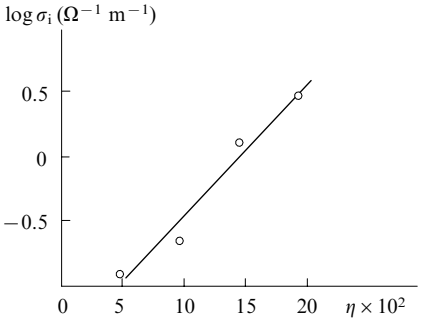


Figure 18. Ionic conductivity with respect to oxygen of the composites Bi_2CuO_4–$n\,Bi_2O_3$ (n = 5 mass %, 10 mass %, 15 mass %, 20 mass %) with the liquid-channel grain-boundary structure *vs.* the volume fraction of the liquid phase at 800 °C.[55]

channel grain-boundary structure may substantially influence the transport properties of the composite.

The dependence of oxygen ion conductivity (σ_i) on the volume fraction of the liquid phase (η) for composites with liquid-channel grain-boundary structure is shown in Fig. 18 . The ionic conductivity increases with increasing volume fraction of the liquid phase. Particularly, oxygen ionic conductivity at $\eta = 0.2$ amounts to $3.2 \times 10^{-2}\ \Omega^{-1}\,cm^{-1}$. High oxygen ion conductivity of composites with liquid-channel grain-boundary structure is due to the presence of liquid matrix in them. Thus, due to the formation of continuous liquid channels in the oxide layer formed during the catastrophic oxidation of copper in contact with Bi_2O_3, its diffusion permeability with respect to oxygen can significantly increase. The copper oxidation rate increases with the increase of the volume fraction of the liquid phase in the oxide layer.

Super-fast stage of catastrophic oxidation of copper

Oxidation of copper under thick (10–30 mm) layers of Bi_2O_3 was analysed in a number of studies.[2, 3, 5, 52] It was found that 0.2–1 mm-thick copper plates are oxidized super-fast (within 5–10 s) upon Bi_2O_3 melting (820 °C), and simultaneously Bi_2O_3 is reduced to metallic bismuth. Copper undergoes super-fast oxidation in air if the mass of bismuth oxide ($m_{Bi_2O_3}$) exceeds 20 times the mass of copper (m_{Cu}). The critical ratio $m_{Bi_2O_3} : m_{Cu}$ decreases with decreasing oxygen partial pressure (Fig. 19). For instance, copper is oxidized super-fast at $m_{Bi_2O_3} : m_{Cu} = 3.6$ if $p_{O_2} = 10^{-2}$–10^2 Pa.

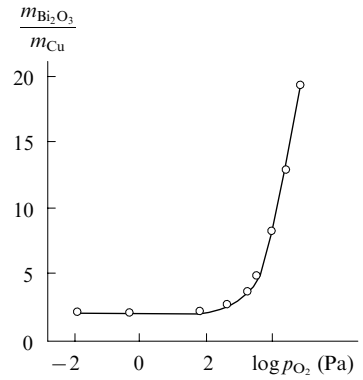


Figure 19. Critical $m_{Bi_2O_3} : m_{Cu}$ ratio *vs.* the oxygen partial pressure.[52]

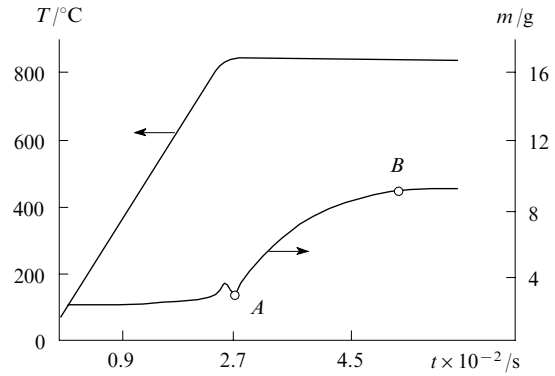


Figure 20. Kinetics of catastrophic oxidation of copper under thick layer of Bi_2O_3 in air.[52]
$m_{Bi_2O_3}$ = 2.226 g, m_{Cu} = 0.036 g.

The kinetic curve of catastrophic oxidation of copper under a thick layer of Bi_2O_3 in air is shown in Fig. 20. At the melting point of Bi_2O_3 (point *A*), an anomalous deviation from the monotonic mass increase is observed. If the process is terminated at point *A*, no copper is detected in the oxidation product but there are granules of metallic bismuth and Bi_2O_3 and Cu_2O phases, and also a minor amount of Bi_2CuO_4. The final oxidation product (point *B*) consists of Bi_2O_3, Bi_2CuO_4 and minor amounts of Cu_2O and CuO. Thus, super-fast oxidation of copper occurs at point *A* according to the equation

$$6\,Cu + Bi_2O_3 \longrightarrow 3\,Cu_2O + 2\,Bi \qquad (12)$$

The mass increase in the region *AB* is due to oxidation of bismuth to Bi_2O_3 and also, in part, of Cu_2O to CuO by atmospheric oxygen.

The microstructure of the product of super-fast copper oxidation under thick layer of bismuth oxide is shown in Fig. 21. Two components are readily discerned, Bi_2O_3 (grey) and Cu_2O (light). Metallic bismuth is present in the oxidation product as granules. The masses of reactants and products are given in Table 3. It can be seen that super-fast oxidation of copper occurs if $m_{Bi_2O_3} : m_{Cu} \geqslant 3.6$.

The super-fast oxidation of copper under thick layer of Bi_2O_3 melt at $p_{O_2} = 10^{-7}$–10^{-3} atm can be explained in the following way. The mass ratio $m_{Bi_2O_3} : m_{Cu} = 3.6$ (or

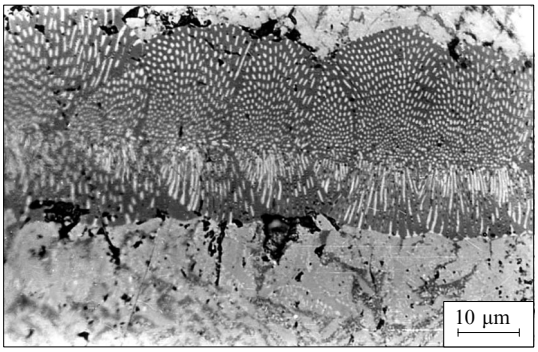


Figure 21. Micrograph of products of catastrophic oxidation of copper under the Bi_2O_3 thick layer.[52]
p_{O_2} = 1 Pa, $m_{Bi_2O_3} : m_{Cu}$ = 3.6, T = 820 °C.

Table 3. Masses (g) of the starting reactants and final products formed upon copper oxidation (T = 820 °C and p_{O_2} = 10 Pa) under a thick layer of Bi_2O_3.[5]

$m_{Bi_2O_3}$	m_{Cu}	m_{Bi} (see [a])	m_{Bi} (see [b])	m_{Cu} (see [c])	$m_{Bi_2O_3} : m_{Cu}$ (see [d])
3.262	0.384	0.418	0.420	0	8.49
3.329	0.548	0.597	0.607	0	6.02
3.106	0.640	0.696	0.698	0	4.85
3.047	0.738	0.803	0.795	0	4.13
3.475	0.960	1.050	1.045	0	3.60
3.475	1.200	1.050	1.050	0.2	2.90

[a] Calculation according to reaction (12). [b] Experiment. [c] The residue (experimental). [d] The initial ratio.

60 mol.% Cu_2O and 40 mol.% Bi_2O_3, taking into account that copper is oxidized to Cu_2O and the content of Bi_2O_3 in the mixture decreases) in the phase diagram of the Bi_2O_3 – Cu_2O system (Fig. 22) at the Bi_2O_3 melting point (820 °C) corresponds to point C of the liquidus. If $m_{Bi_2O_3} : m_{Cu} > 3.6$, the virtual point lies above the liquidus, copper is oxidized to Cu_2O, which continuously dissolves in the melt. Therefore the super-fast oxidation of copper occurs on a permanently exposed metallic surface (having no protective oxide layer). If $m_{Bi_2O_3} : m_{Cu} < 3.6$, a part of copper equal to 1 : 3.6 of the Bi_2O_3 mass undergoes super-fast oxidation, then the virtual point shifts below the liquidus to the two-phase region, where solid Cu_2O and the melt are in equilibrium. A solid Cu_2O layer containing the liquid phase is formed on copper surface in the course of subsequent oxidation, which proceeds according to diffusion mechanism (the fast stage).

The super-fast oxidation of copper is also observed at $p_{O_2} > 10^2$ Pa; however, the critical ratio of the bismuth oxide mass to the copper mass sharply increases under these conditions (see Fig. 19). In this case, the mechanism of super-fast oxidation of copper does not basically differ from the mechanism described above with the only exception that CuO is thermodynamically stable at $p_{O_2} \approx 6 \times 10^3$ Pa, and the formation of Bi_2CuO_4 accompanied by a decrease in the amount of starting Bi_2O_3 is possible. The minor decrease in the mass in the kinetic curve of copper oxidation (see Fig. 20, point *A*) is, probably, due to incongruent melting of Bi_2CuO_4.[107]

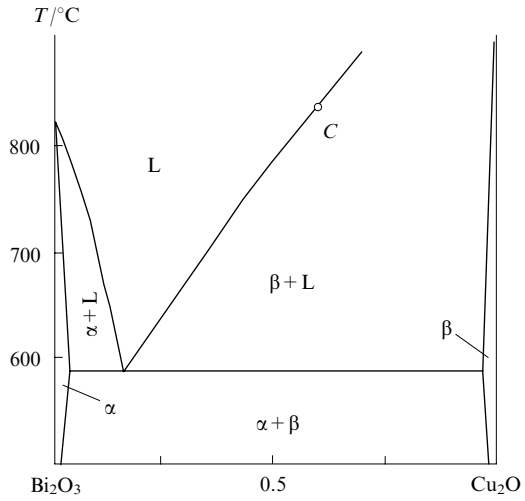


Figure 22. Phase diagram of the Bi_2O_3 – Cu_2O system.[52]

Thus, super-fast oxidation of copper is related to the permanent dissolution of the protective oxide layer in the melt and occurs on exposed metallic surface according to Eqn (12). The critical ratio $m_{Bi_2O_3} : m_{Cu}$ at which super-fast oxidation of copper occurs is determined by location of the virtual point in the liquidus of the Bi_2O_3 – Cu_2O state diagram corresponding to the Bi_2O_3 melting point (820 °C).

Catastrophic oxidation of copper in contact with Bi_2O_3 can proceed according to both the diffusion mechanism (the fast stage) and the mechanism involving dissolution of a protective oxide layer (super-fast stage). Depending on the ratio of masses of copper and low-melting oxide, one or another mechanism is implemented. In the case of catastrophic copper oxidation, the diffusion mechanism operates if copper is coated by a thin layer (< 100 μm) of low-melting oxide and the solution mechanism is realized if copper is coated by a thick layer (> 1 cm).

b. The Cu – MoO_3 and Cu – V_2O_5 systems

The fast stage of catastrophic oxidation of copper

The kinetics of catastrophic oxidation of copper in contact with MoO_3 and V_2O_5 was studied by Klimashin and Belousov.[56, 57, 112, 113] The kinetic curves for oxidation of copper precoated by MoO_3 at 500, 600 and 700 °C in air are shown in Fig. 23. The coated copper is catastrophically oxidized at 480 °C. The copper oxidation rate increases with increasing the specific weight of the coating (curves *2* – *4* in Fig. 23 *a* – *c*).

The kinetics curves for oxidation of copper coated by a V_2O_5 layer are shown in Fig. 23 *d* – *f*. In this case, copper is catastrophically oxidized at 560 °C. The copper oxidation rate also increases with increasing specific weight of the coating (curves *2*, *3* and *4* in Fig. 23 *d* – *f*).

The threshold temperatures for catastrophic oxidation of copper in the Cu – MoO_3 and Cu – V_2O_5 systems (480 °C and 560 °C, respectively) coincide with the melting points of the eutectics between Cu_2O and MoO_3 and between Cu_2O and V_2O_5, respectively (Fig. 24).

The typical microstructure of the oxide layer formed in the catastrophic oxidation of copper in contact with MoO_3 (or V_2O_5) in air is demonstrated by micrographs shown in Figs 25 and 26. Transverse through channels consisting of

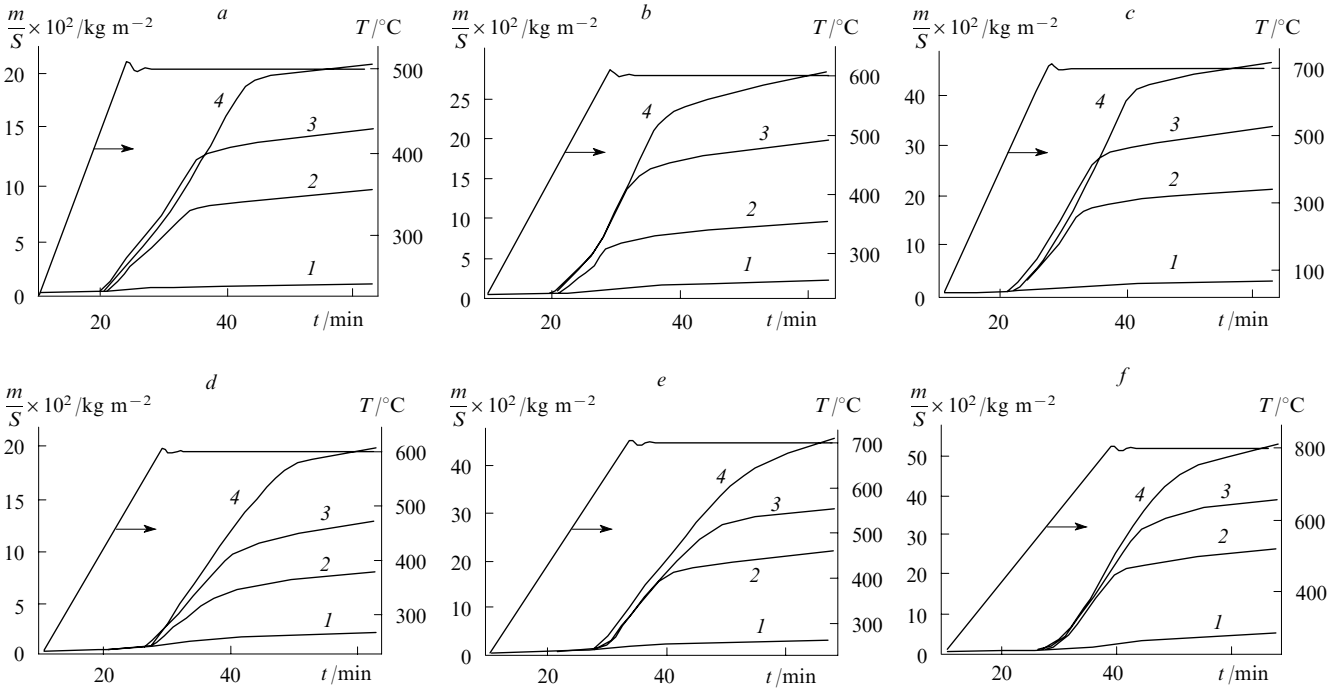


Figure 23. Kinetics of oxidation of copper in contact with MoO_3 (*a*–*c*) and V_2O_5 (*d*–*f*) in air at 500 (*a*), 600 (*b*, *d*), 700 (*c*, *e*) and 800 °C (*f*).[56]
(*a*–*c*): Specific weight of MoO_3/kg m^{-2}: 0 (no coating) (*1*), 0.3 (*2*), 0.6 (*3*), 0.9 (*4*);
(*d*–*f*): specific weight of V_2O_5/kg m^{-2}: 0 (no coating) (*1*), 0.075 (*2*), 0.15 (*3*), 0.0225 (*4*).

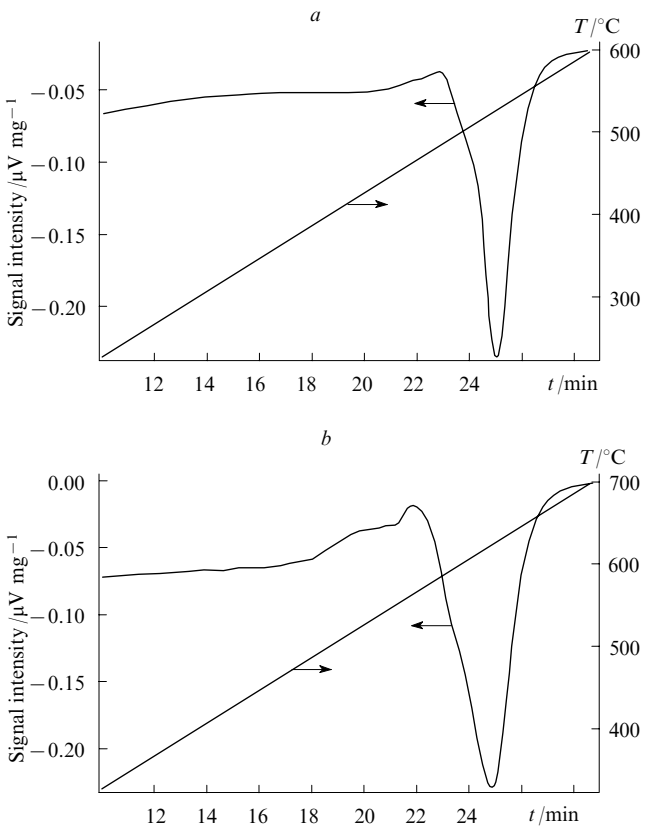


Figure 24. DTA plots for powders of Cu_2O–50 mass % MoO_3 (*a*) and Cu_2O–50 mass % V_2O_5 (*b*) at p_{O_2} = 0.2 Pa.[56,57]

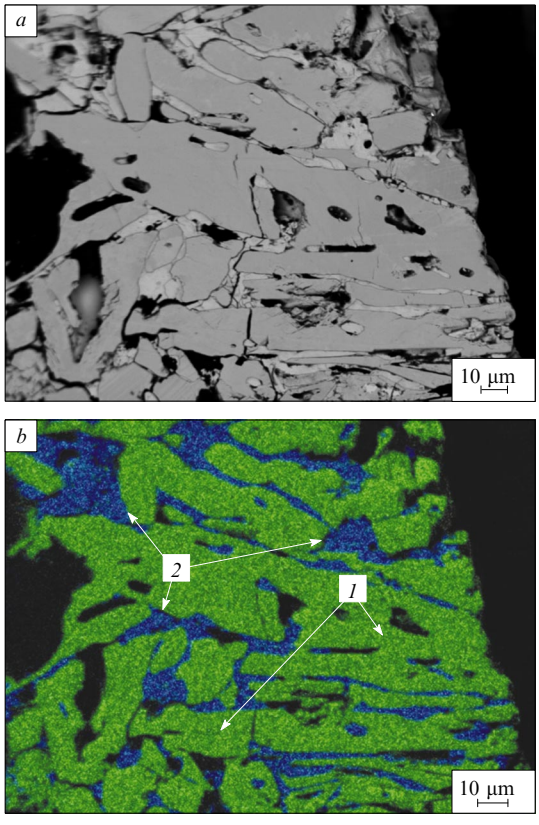


Figure 25. Micrographs of the oxide layer formed in the catastrophic oxidation of copper in contact with MoO_3 at 600 °C (*a*) and distribution of copper (*1*) and molybdenum (*2*) in the layer (*b*).[56] The specific weight of MoO_3 is 0.9 kg m^{-2}.

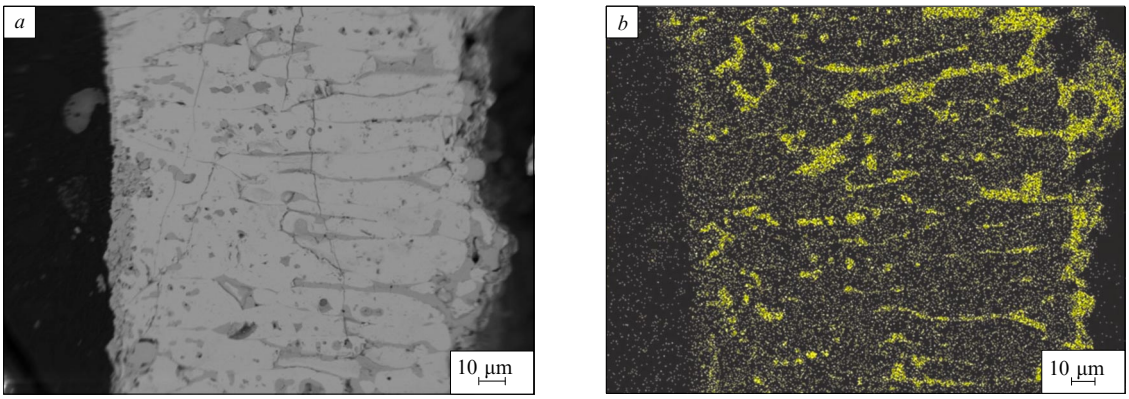


Figure 26. Micrographs of the oxide layer formed in the catastrophic oxidation of copper in contact with V_2O_5 at 700 °C (*a*) and distribution of vanadium in the layer (*b*).[57] The specific weight of V_2O_5 is 0.225 kg m^{-2}.

Cu_2O, MoO_3 (or V_2O_5) and mixed oxide $Cu_3Mo_2O_9$ (or Cu_3VO_4) are seen. The rest of the layer is formed by Cu_2O and CuO.

A micrograph of the transverse channels is shown in Fig. 27. A typical eutectic is seen in the micrographs. This indicates that the transverse channels were liquid during catastrophic oxidation. The liquid channels may serve to transport ions of oxygen or copper because diffusion coefficients in melts are larger than in solids.

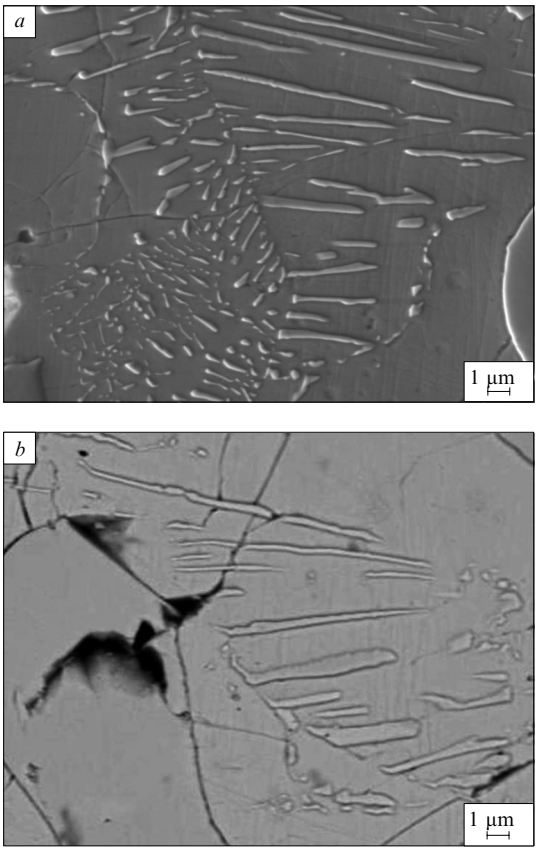


Figure 27. Micrographs of transverse channels in the oxide layers shown in Fig. 25 *a* (*a*) and 26 *a* (*b*).[56, 57]

Transport properties of model $MoO_3-CuMoO_4$ and $V_2O_5-CuV_2O_6$ composites

To determine the role of the liquid phase in the catastrophic oxidation of copper in contact with low-melting oxides MoO_3 and V_2O_5, the permeability of model composites MoO_3–(8–11) mass % $CuMoO_4$ and V_2O_5–(12–18) mass % CuV_2O_6 with respect to oxygen was measured by gas chromatography both below (the solid phases) and above the solidus temperature (in the two-phase region of the state diagram where the solid and liquid phases are in equilibrium).[56, 57] The choice of these phases was dictated by availability of their phase diagrams,[114, 115] which enabled targeted variation of the volume fraction of the liquid phase in the composites at temperatures above the eutectic points, which are 710 °C for the $MoO_3-CuMoO_4$ system and 630 °C for the $V_2O_5-CuV_2O_6$ system.

High permeability of the composites with respect to oxygen was only detected at and above the eutectic point. The oxygen permeability below the eutectic point (when the phase is solid) was not revealed. The results of measurements of oxygen flux (J) through composites, including solid oxide and melt depending on the volume fraction of the liquid phase are shown in Figs 28 and 29. The oxygen flux through these composites increases with the increase in the volume fraction of the liquid phase and amounts to 1.7×10^{-4} mol m^{-2} s^{-1} for MoO_3–11 mass % $CuMoO_4$ ($\eta\approx25$ vol.%) at 710 °C and 1.6×10^{-4} mol m^{-2} s^{-1} for V_2O_5–18 mass % CuV_2O_6 ($\eta\approx30$ vol.%) at 630 °C.

In accordance with the Wagner equation,[1] the specific oxygen flux through these composites is expressed as follows:

$$J=\frac{RT}{16LF^2}\sigma_{amb}\ln\frac{p''_{O_2}}{p'_{O_2}} \qquad (13)$$

where R is the universal gas constant, L is thickness of the sample, F is the Faraday constant, p''_{O_2} and p'_{O_2} are partial oxygen pressures on the opposite sides of the composite ($p''_{O_2}\ll p'_{O_2}$), σ_{amb} is ambipolar conductivity

$$\sigma_{amb}=\frac{\sigma_i\,\sigma_e}{\sigma_i+\sigma_e} \qquad (14)$$

σ_i is oxygen ionic conductivity, σ_e is electronic conductivity.

If $\sigma_e\gg\sigma_i$, Eqn (14) is transformed to the form $\sigma_{amb}=\sigma_i$. This equation is valid for high-temperature oxidation of copper when a solid oxide layer is formed on

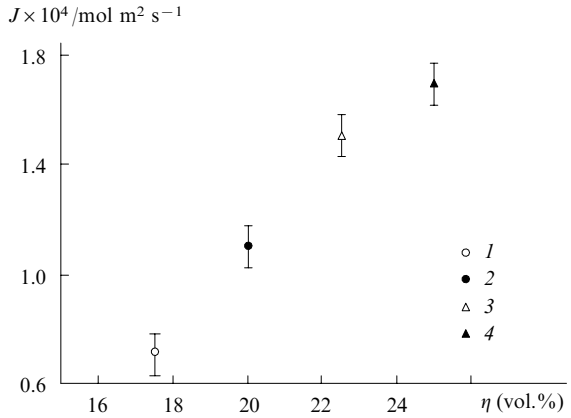


Figure 28. Dependence of the specific oxygen flux on the volume fraction of the liquid phase in the $MoO_3 - n\,CuMoO_4$ composites at 720 °C.[56]
n (mass %): 8 (*1*), 9 (*2*), 10 (*3*), 11 (*4*).

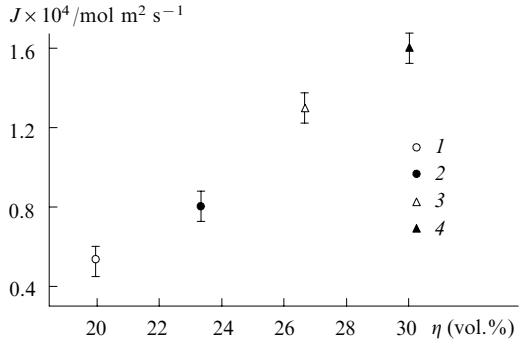


Figure 29. Dependence of the specific oxygen flux on the volume of the liquid phase in the $V_2O_5 - n\,CuV_2O_6$ composites at 640 °C.[57]
n (mass %): 12 (*1*), 14 (*2*), 16 (*3*), 18 (*4*).

its surface. If an oxide layer containing the liquid phase is formed on the copper surface, its ionic conductivity may be of the same order of magnitude as the electronic conductivity,[116–124] then Eqn (14) is applicable. The rate of catastrophic oxidation of copper is limited by ambipolar conductivity for oxygen ions and electrons, *i.e.*, by associated diffusion of oxygen ions along liquid channels and transport of electrons in both the liquid and solid phases.[122, 123]

On the basis of the presented experimental data, it is possible to conclude that formation of transverse liquid channels in the oxide layer leads to the substantial increase in its diffusion permeability for oxygen, this results in the sharp increase of the rate of copper oxidation. The greater the volume fraction of the liquid phase in the oxide layer, the higher the rate of oxidation of copper.

Reactions in the Cu–MoO_3 and Cu–V_2O_5 systems

During catastrophic oxidation of copper in contact with MoO_3 or V_2O_5, redox reactions can proceed at the copper/oxide layer interface where partial oxygen pressure is reduced. Studies of the reactions in the Cu–MoO_3 and Cu–V_2O_5 systems at 795 °C and 670 °C (at the melting points of MoO_3 and V_2O_5, respectively) and $p_{O_2} = 0.2$ Pa have demonstrated[56, 57] that the following reactions occur in these systems

$$2\,Cu + MoO_3 \longrightarrow Cu_2O + MoO_2 \quad (15)$$

$$2\,Cu + V_2O_5 \longrightarrow Cu_2O + 2\,VO_2 \quad (16)$$

Thermodynamic calculations[125] also confirm that these reactions are possible.

Rate constants

The kinetic curves for catastrophic oxidation of copper (see Fig. 23) are straight lines in parabolic coordinates (Fig. 30). This means that the catastrophic oxidation of copper follows a parabolic time law. The rate of the process is determined by associated diffusion of oxygen ions along liquid channels in the oxide layer and electrons in both the liquid and solid phases.[126]

Parabolic rate constants for catastrophic oxidation of copper obtained by formula (11) from the data presented in Fig. 30 are summarized in Table 4. The parabolic rate constant of catastrophic oxidation of copper coated by MoO_3 or V_2O_5 increases with the increase in the specific weight of the latter and can exceed the parabolic rate constant for high-temperature oxidation of uncoated copper by two orders of magnitude.

Table 4. Parabolic rate constants for catastrophic oxidation of copper in contact with MoO_3 or V_2O_5.[112, 113, 125]

$\frac{m_{MoO_3}}{S}$ (see [a])	T/°C	k'' (see [b])	$\frac{m_{V_2O_5}}{S}$ (see [a])	T/°C	k'' (see [b])
0	500	2.5×10^{-8}	0	600	1.0×10^{-7}
0.3	500	9.3×10^{-7}	0.075	600	9.8×10^{-7}
0.6	500	1.9×10^{-6}	0.15	600	2.7×10^{-6}
0.9	500	2.3×10^{-6}	0.225	600	4.5×10^{-6}
0	600	1.0×10^{-7}	0	700	2.9×10^{-7}
0.3	600	3.1×10^{-6}	0.075	700	3.4×10^{-6}
0.6	600	6.5×10^{-6}	0.15	700	8.6×10^{-6}
0.9	600	1.0×10^{-5}	0.225	700	1.6×10^{-5}
0	700	2.9×10^{-7}	0	800	1.0×10^{-6}
0.3	700	9.2×10^{-6}	0.075	800	9.7×10^{-6}
0.6	700	2.1×10^{-5}	0.15	800	2.2×10^{-5}
0.9	700	3.8×10^{-5}	0.225	800	4.1×10^{-5}

[a] In kg m^{-2}. [b] In kg^2 m^{-4} s^{-1}

The temperature dependences of parabolic rate constants for catastrophic oxidation of copper in the Cu–MoO_3 and Cu–V_2O_5 systems are shown in Fig. 31. The activation energies were obtained with the use of these dependences.

The activation energies for the Cu–MoO_3 system are the following:

$\frac{m_{MoO_3}}{S}$/kg m^{-2}	0.3	0.6	0.9
E_a/kJ mol^{-1}	71.5	74.9	87.5

The activation energies for the Cu–V_2O_5 system are the following:

$\frac{m_{V_2O_5}}{S}$/kg m^{-2}	0.075	0.150	0.225
E_a/kJ mol^{-1}	89.3	80.0	86.2

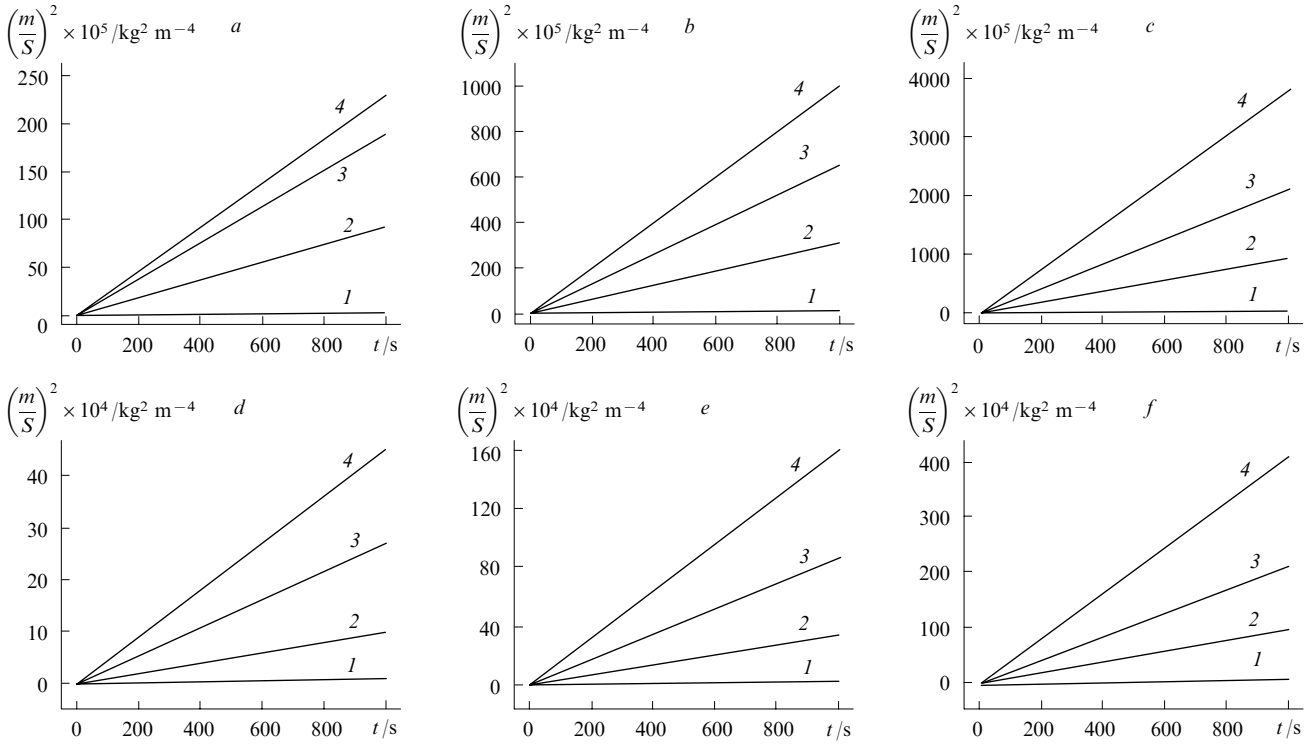


Figure 30. Kinetics of oxidation of copper in contact with MoO_3 (*a*–*c*) and V_2O_5 (*d*–*f*) in air at 500 (*a*), 600 (*b*, *d*), 700 (*c*, *e*) and 800 °C (*f*);[56, 57]
(*a*–*c*): Specific weight of MoO_3 /kg m^{-2}: 0 (no coating) (*1*), 0.3 (*2*), 0.6 (*3*), 0.9 (*4*);
(*d* –*f*): specific weight of V_2O_5 /kg m^{-2}: 0 (no coating) (*1*), 0.075 (*2*), 0.15 (*3*), 0.225 (*4*).

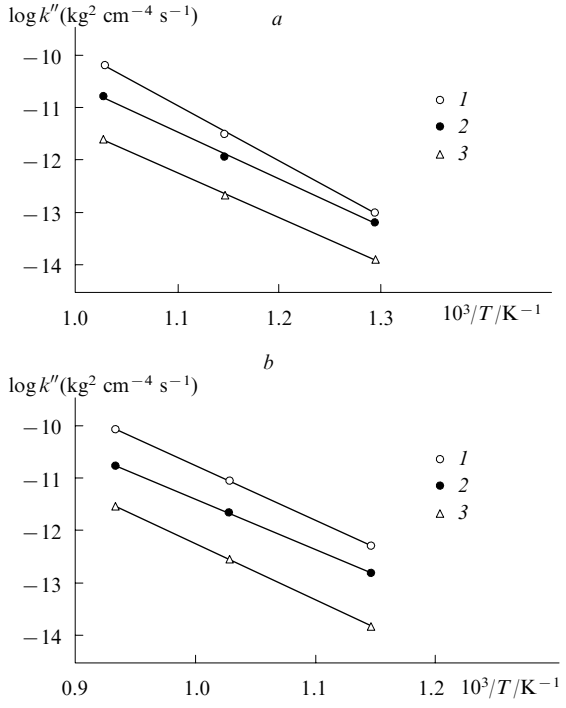


Figure 31. Temperature dependences of the parabolic rate constant for catastrophic oxidation of copper in contact with MoO_3 (*a*) and V_2O_5 (*b*).[56, 57]
(*a*): Specific weight of MoO_3 /kg m^{-2}: 0.9 (*1*), 0.6 (*2*), 0.3 (*3*);
(*b*): specific weight of V_2O_5 /kg m^{-2}: 0.225 (*1*), 0.15 (*2*), 0.075 (*3*).

2. Model of catastrophic oxidation of copper under thin layer of low-melting oxide

Before turning to the quantitative description of the catastrophic oxidation of copper in contact with low-melting oxides, we formulate the key points of the model:

— continuous transverse liquid channels are formed in the oxide layer during catastrophic oxidation of copper;

— the liquid channels serve as diffusion paths for oxygen ions;

— at the metal/oxide interface, copper reacts with low-melting oxide according to reactions (12), (15) or (16);

— the reaction products are oxidized by air oxygen, which is transported along the liquid channels;

— the diffusion of oxygen ions along the liquid channels is the rate-limiting step of the process;

— oxygen ions and electrons are the major charge carriers;

— the oxide layer thickness is much greater than the distance by which the space charge can act (electrical double layer).

Suppose that at time t the thickness of the oxide layer on copper is h (Fig. 32). If oxygen concentration in the oxide layer is c^*, the equation of the mass balance takes the following form:

$$c^* \frac{\mathrm{d}h}{\mathrm{d}t} = J \qquad (17)$$

where J is the oxygen flux through the effective cross-section of the liquid phase in the oxide layer.

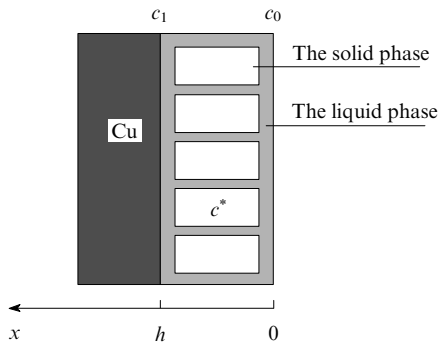


Figure 32. Schematic view of the oxide layer formed on the copper surface during catastrophic oxidation.

In accordance with Fick's first law, the flux is expressed as follows:

$$J = -D_{\text{ef}} \frac{\mathrm{d}c}{\mathrm{d}x} \tag{18}$$

where D_{ef} is an effective diffusion coefficient for oxygen ions in the oxide layer

$$D_{\text{ef}} = D_{\text{i}}\,\eta \tag{19}$$

D_{i} is diffusion coefficient for oxygen ions in the liquid phase, η is the volume fraction of the liquid phase in the oxide layer.

By substituting the oxygen flux expressed by Eqns (18) and (19) into the right-hand part of Eqn (17), one gets

$$c^* \frac{\mathrm{d}h}{\mathrm{d}t} = -D_{\text{i}}\,\eta \frac{\mathrm{d}c}{\mathrm{d}x} \tag{20}$$

If we assume that a steady state is established at the oxide layer/air and copper/oxide layer interfaces, then the diffusion of oxygen occurs at constant boundary conditions $c_{x=0,\,t} = c_0$ and $c_{x=h,\,t} = c_1$. Assuming a linear change in the concentration of oxygen ions in the liquid channel, we obtain

$$\frac{\mathrm{d}c}{\mathrm{d}x} = \frac{c_1 - c_0}{h} \tag{21}$$

If the oxygen ion concentration c_1 is taken to be zero (as it is very low), then expression (21) is transformed to the form

$$\frac{\mathrm{d}c}{\mathrm{d}x} = -\frac{c_0}{h} \tag{22}$$

By substituting Eqn (22) into (20), one obtains

$$c^* \frac{\mathrm{d}h}{\mathrm{d}t} = D_{\text{i}}\,\eta \frac{c_0}{h} \tag{23}$$

Separation of the variables in Eqn (23) and integration

$$c^* \int_0^h h\mathrm{d}h = D_{\text{i}}\,\eta c_0 \int_0^t \mathrm{d}t \tag{24}$$

gives a parabolic time law for oxidation

$$h^2 = k' t \tag{25}$$

where k' is the parabolic rate constant for oxidation of copper

$$k' = \frac{2D_{\text{i}}\,\eta c_0}{c^*} \tag{26}$$

The constants k'' (kg^2 m^{-4} s^{-1}) and k' (m^2 s^{-1}) are related by the following equation:

$$k'' = \rho^2 k' \tag{27}$$

where ρ is the density of the oxide layer.

By substituting the expression for k' (26) into Eqn (27), one obtains

$$k'' = \frac{2D_{\text{i}}\,\rho^2 \eta c_0}{c^*} \tag{28}$$

The density of the oxide layer and the oxygen concentration in the layer can be assumed to be equal to these values for Cu_2O ($\rho = 6 \times 10^3$ kg m^{-3}, $c^* = 4.2 \times 10^4$ mol m^{-3}). According to the data of a publication,[127] diffusion coefficient and concentration of dissolved oxygen in metal oxide melts are $D_{\text{i}} \approx 5 \times 10^{-9}$ m^2 s^{-1}, $c_0 \approx$ 10 mol m^{-3}.

The parabolic rate constants for catastrophic oxidation of copper in contact with MoO_3 or V_2O_5, calculated by Eqn (28) with the use of experimental data on the volume fraction of the liquid phase in the oxide layer (see Figs 25 and 26) and obtained experimentally are of the same order of magnitude (Table 5). Thus, the theory agrees with experiment.

Table 5. Calculated and experimentally obtained parabolic rate constants for catastrophic oxidation of copper in contact with MoO_3 and V_2O_5.[127]

$\frac{m_{\text{Ox}}}{S}$/kg m^{-2} (see [a])	T/°C	η	$k'' \times 10^5$/kg^2 m^{-4} s^{-1}	
			experiment	calculations
Oxidation of copper in contact with MoO_3				
0.9	600	0.16	1.0	1.4
0.9	700	0.25	3.8	2.2
Oxidation of copper in contact with V_2O_5				
0.225	700	0.14	1.6	1.2
0.225	800	0.27	4.1	2.3

[a] m_{Ox} is the specific weight of the oxide.

* * *

It can be concluded from the above discussion that the process of high-temperature oxidation of copper is a diffusion-controlled process. The rate of the high-temperature oxidation of copper is determined by the bulk diffusion of copper cations in solid Cu_2O. The process of catastrophic copper oxidation may occur both in diffusion (the fast stage) and in kinetic (super-fast stage) regimes. In the first case, the rate of catastrophic oxidation of copper is deter-

mined by the diffusion of oxygen anions in the liquid phase, while in the second case, it is determined by dissolution of the Cu_2O protective oxide layer.

Lately, the concepts concerning the processes of accelerated charge and mass transfer with participation of liquid phases in oxide layers formed on metal surfaces during catastrophic oxidation have been markedly extended.[126] This greatly influenced the development of, for example, membrane science. For instance, new ion transport membranes possessing highly selective oxygen permeability were developed [122 – 124, 128 – 133] on the basis of composites with the liquid-channel grain-boundary structure; they represent an alternative to traditional ceramic membranes. Nevertheless, there is a number of unsolved problems in this area. One challenge is to ascertain the mechanisms of oxygen ion and electron transport in metal oxide melts.[134, 135] Another important problem consists in the development of a quantitative theory of ion transport in the solid oxide/melt interfaces. The solution of these fundamental problems will significantly contribute to the understanding of the catastrophic oxidation of metals and to the development of materials for effective metal protection.

References

1. J R Davis *Copper and Copper Alloys* (Materials Park, OH: ASM International Handbook Committee, 2001)
2. V V Belousov *Oxid. Met.* **42** 511 (1994)
3. V V Belousov *Zashch. Met.* **30** 599 (1994) [a]
4. C Wagner *Z. Phys. Chem. B* **21** 25 (1938)
5. V V Belousov *Rus. J. Phys. Chem. A* **82** 79 (2008)
6. T P Gabb, J Telesman, B Hazel, D P Mourer *J. Mater. Eng. Perform.* **19** 77 (2010)
7. C L Zeng, Z J Feng, Y Liu *Oxid. Met.* **76** 83 (2011)
8. S-H Cho, S-S Hong, D-S Kang, J-M Hur, H-S Lee *Met. Mater. Int.* **15** 51 (2009)
9. F Pettit *Oxid. Met.* **76** 1 (2011)
10. R Kumar, V K Tewari, S Prakash *Met. Mater. Trans. A* **38** 54 (2007)
11. Y Xiong, C Guan, S Zhu, F Wang *J. Mater. Eng. Perform.* **15** 564 (2006)
12. M Li, X Sun, W Hu, H Guan, S Chen *Oxid. Met.* **65** 137 (2006)
13. S Kamal, R Jayaganthan, S Prakash *Bull. Mater. Sci.* **33** 299 (2010)
14. R Kumar, V K Tewari, S Prakash *J. Mater. Eng. Perform.* **18** 959 (2009)
15. N Birbilis, R G Buchheit *Met. Mater. Trans. A* **39** 3224 (2008)
16. W M Lu, T J Pan, Y Niu *Oxid. Met.* **69** 63 (2008)
17. K Chandra, V Kain, G K Dey *J. Fail. Anal. Prev.* **11** 466 (2011)
18. W M Lu, T J Pan, K Zhang, Y Niu *Corros. Sci.* **50** 1900 (2008)
19. W Li, Y Liu, Y Wang, Ch Han, H Tang *Trans. Nonferrous Met. Soc. China* **21** 2617 (2011)
20. G M Liu, F Yu, J H Tian, J H Ma *Mater. Sci. Eng. A* **496** 40 (2008)
21. M Anuwar, R Jayaganthan, V K Tewari, N Arivazhagan *Mater. Lett.* **61** 1483 (2007)
22. X Yang, X Peng, F Wang *Scr. Mater.* **56** 891 (2007)
23. C L Zeng, J Li *Electrochim. Acta* **50** 5533 (2005)
24. M N Task, B Gleeson, F S Pettit, G H Meier *Surf. Coat. Technol.* **206** 1552 (2011)
25. Z-G Liu, J-H Ouyang, Y Zhou, S Li *J. Eur. Ceram. Soc.* **30** 2707 (2010)
26. L-C Chen, C Zhang, Z-G Yang *Corros. Sci.* **53** 374 (2011)
27. A Magdziarz, Z Kalicka *Corros. Sci.* **49** 1869 (2007)
28. J G González-Rodriguez *Corros. Sci.* **51** 1420 (2009)
29. S-H Cho, J-M Hur, C-S Seo, J-S Yoon, S-W Park *J. Alloys Compd.* **468** 263 (2009)
30. V V Belousov, A A Klimashin *Met. Mater. Trans. A* **43** 3715 (2012)
31. R A Rapp *Corrosion* **42** 568 (1986)
32. R A Rapp *Pure Appl. Chem.* **62** 113 (1990)
33. F S Pettit, C S Giggins *Hot Corrosion in Superalloys* (Eds C T Sims, N S Stoloff, W C Hagel) (New York: Wiley, 1987)
34. S R J Saunders, in *Guidelines for Methods of Testing and Research in High Temperature Corrosion* (Eds H J Grabke, D B Meadowcroft) (London: Institute of Materials, 1995)
35. D A Shifler, in *High Temperature Gaseous Corrosion Testing* (Materials Park, Columbus, OH: ASM Handbook, 2003) Vol. 13A, p. 650
36. P D Jose, D K Gupta, R A Rapp *J. Electrochem. Soc.* **132** 735 (1985)
37. T S Sidhu, S Prakash, R D Agrawal *Curr. Sci.* **90** 41 (2006)
38. M H Li, X F Sun, J G Li, Z Y Zhang, H R Guan, Z Q Hu *Oxid. Met.* **59** 591 (2003)
39. U J Grabke, G H Meier *Oxid. Met.* **44** 147 (1995)
40. A K Misra *Oxid. Met.* **25** 129 (1986)
41. A K Mirsa *J. Electrochem. Soc.* **133** 1038 (1986)
42. N Eliaz, G Shemesh, R M Latanision *Eng. Fail. Anal.* **9** 31 (2002)
43. Y Zhang, R A Rapp *Corrosion* **43** 348 (1987)
44. Y S Huang, R A Rapp *Corrosion* **45** 933 (1989)
45. H Singh, D Puri, S Prakash *Rev. Adv. Mater. Sci.* **16** 27 (2007)
46. M A Uusitalo, P M J Vuoristo, T A Mantyla *Mater. Sci. Eng. A* **346** 168 (2003)
47. H Singh, D Puri, S Prakash *Surf. Coat. Technol.* **192** 27 (2005)
48. W-M Zhao, Y Wang, L-X Dong, K-Y Wu, J Xue *Surf. Coat. Technol.* **190** 293 (2005)
49. B S Sidhu, S Prakash *Surf. Coat. Technol.* **166** 89 (2003)
50. Q M Wang, Y N Wu, P L Ke, H T Cao, J Gong, C Sun, L S Wen *Surf. Coat. Technol.* **186** 389 (2004)
51. R A Rapp *Corros. Sci.* **44** 209 (2002)
52. V V Belousov *Oxid. Met.* **67** 235 (2007)
53. P Kofstad *High Temperature Corrosion* (Amsterdam: Elsevier, 1988)
54. V V Belousov *Russ. Chem. Rev.* **67** 563 (1998)
55. V V Belousov *Corros. Sci.* **52** 68 (2010)
56. A A Klimashin, V V Belousov *Corros. Sci.* **53** 3150 (2011)
57. A A Klimashin, V V Belousov *Oxid. Met.* **76** 359 (2011)
58. C Wagner, H Hammen *Z. Phys. Chem. B* **40** 197 (1938)
59. F A Kröger *The Chemistry of Imperfect Crystals* (Amsterdam: North Holland, 1964)
60. G M Raynaud, W A T Clark, R A Rapp *Met. Trans. A* **15** 573 (1984)
61. O Kubaszewski, B E Hopkins *Oxidation of Metals and Alloys* (London: Butterworths, 1962)
62. K Hauffe *Reaktione in und an Festen Stoffen* (Berlin: Springer, 1966)
63. K Hauffe *Oxydation von Metallen und Metallegierungen* (Berlin: Springer, 1956)
64. H Dunwald, C Wagner *Z. Phys. Chem. B* **17** 467 (1932)
65. J Günderman, K Hauffe, K Wagner *Z. Phys. Chem. B* **37** 148 (1937)
66. R F Tylecote *J. Inst. Met.* **78** 259 (1950)
67. R F Tylecote *J. Inst. Met.* **81** 681 (1952)
68. W M McKewan, W M Fassel *J. Met.* **5** 1127 (1953)
69. S Mrowec, A Stoclosa *Oxid. Met.* **3** 291 (1971)
70. R F Tylecote *J. Inst. Met.* **78** 327 (1950)
71. D W Bridges, J P Baur, W M Fassel *J. Electrochem. Soc.* **103** 273 (1956)
72. L Czerski, S Mrowec, T Werber *Roczniki Chem.* **38** 643 (1964)
73. J H Park, K Natesan *Oxid. Met.* **39** 411 (1993)
74. P Kofstad *High-Temperature Oxidation of Metals* (Wiley: New York, 1966)
75. J A Sartell, C H Li *Trans. Am. Soc. Met.* **55** 158 (1962)

76. G Valensi, in *Pittsburgh International Conference of Surface Reactions, Pittsburgh, 1948* p. 156
77. N Birks, G H Meier, F S Pettit *Introduction to the High-Temperature Oxidation of Metals* (Cambridge: Cambridge University Press, 2006)
78. M Honkanen, M Vippola, T Lepisto *J. Mater. Sci.* **42** 4684 (2007)
79. O Kubaschewski, O V Goldbeck *Z. Metallkd.* **39** 158 (1946)
80. C Gench, K Hauffe *Z. Phys. Chem.* **196** 427 (1951)
81. G Valensi *Metallurg. Ital.* **42** 77 (1950)
82. V B Voitovich *Oxid. Met.* **42** 249 (1994)
83. Y Zhu, K Mimura, M Ishiki *Corros. Sci.* **47** 537 (2005)
84. W W Smeltzer, R R Haering, J S Kirkaldy *Acta Metall.* **9** 880 (1961)
85. Y Zhu, M Mimura, M Isshiki *Oxid. Met.* **59** 575 (2003)
86. Y Zhu, K Mimura, M Ishiki *Corros. Sci.* **46** 2445 (2004)
87. J Paidassi *Acta Metall.* **6** 216 (1958)
88. F De Carli, N Collari *Chim. Ind.* **33** 77 (1951)
89. H J Grabke *Mater. Tehnol.* **40** 39 (2006)
90. Y Shima, Y Ishikawa, H Nitta, Y Yamazaki *Matter. Trans.* **43** 173 (2002)
91. D M Smyth *The Defect Chemistry of Metal Oxides* (Oxford: Oxford University Press, 2002)
92. J Maluenda, R Farhi, G Petot-Ervas *J. Phys. Chem. Solids* **42** 911 (1981)
93. J Maluenda, R Farhi, G Petot-Ervas *J. Phys. Chem. Solids* **42** 697 (1981)
94. F Perinet, S Barbezat, C Monty *J. Phys. Colloq. C* **6** 315 (1980)
95. W J Tomlinson, J Yates *J. Phys. Chem. Solids* **38** 1205 (1977)
96. F Biccari, Ph. D. Thesis, Sapienza University, Rome, 2009
97. N L Peterson, C L Wiley *J. Phys. Chem. Solids* **45** 281 (1984)
98. Y Zhu, K Mimura, M Isshiki *Oxid. Met.* **62** 207 (2004)
99. G Garnaud *Oxid. Met.* **11** 127 (1977)
100. G J Yurek, J P Hirth, R A Rapp *Oxid. Met.* **8** 265 (1974)
101. W C Leslie, M G Fontana *Trans. Am. Soc. Met.* **41** 1213 (1949)
102. G W Rathenau, J L Meijering *Nature (London)* **165** 167 (1950)
103. V N Konev, V V Belousov *Zashch. Met.* **25** 138 (1989) [a]
104. V V Belousov *Oxid. Met.* **38** 289 (1992)
105. V V Belousov, B S Bokschtein *Oxid. Met.* **50** 389 (1998)
106. V V Belousov, B S Bokshtein *Zashch. Met.* **34** 36 (1998) [a]
107. B Haltstedt, D Risold, L J Gauckler *J. Am. Ceram. Soc.* **79** 353 (1996)
108. V V Belousov *J. Mater. Sci.* **40** 2361 (2005)
109. V V Belousov *J. Am. Ceram. Soc.* **82** 1342 (1999)
110. N V Lyskov, Yu G Metlin, V V Belousov, Yu D Tretyakov *Dokl. Chem.* **392** 229 (2003)
111. N V Lyskov, Yu G Metlin, V V Belousov, Yu D Tretyakov *Solid State Ionics* **166** 207 (2004)
112. A A Klimashin, V V Belousov *Korroz. Mater. Zashch.* **9** 1 (2011) [a]
113. A A Klimashin, V V Belousov *Materialovedenie* **4** 53 (2011) [b]
114. K Nassau, J W Shiever *J. Am. Ceram. Soc.* **52** 36 (1969)
115. N B Gorilovskaya, N G Chaban, V V Safronov *Zh. Neorg. Khim.* **33** 16 (1988) [c]
116. V V Belousov *J. Am. Ceram. Soc.* **79** 1703 (1996)
117. V V Belousov *Neorg. Mater.* **39** 94 (2003) [d]
118. V V Belousov *Korroz. Mater. Zashch.* **5** 22 (2004) [a]
119. N V Lyskov, Yu G Metlin, V V Belousov, Yu D Tretyakov *Solid State Ionics* **173** 135 (2004)
120. V V Belousov *Kolloid. Zh.* **66** 149 (2004) [e]
121. V V Belousov *Elektrokhimiya* **31** 1343 (1995) [f]
122. S V Fedorov, V V Belousov, A V Vorobiev *J. Electrochem. Soc.* **155** F241 (2008)
123. V V Belousov, S V Fedorov, A V Vorobiev *J. Electrochem. Soc.* **158** B601 (2011)
124. I Kul'bakin, V Belousov, S Fedorov, A Vorobiev *Mater. Lett.* **67** 139 (2012)
125. A A Klimashin, Candidate Thesis in Chemical Sciences, A A Baikov Institute of Metallurgy and Materials Science, Moscow, 2012
126. V V Belousov, S V Fedorov *Russ. Chem. Rev.* **81** 44 (2012)
127. M Sasabe, K S Goto *Metall. Trans. A* **5** 2225 (1974)
128. V V Belousov, V A Schelkunov, S V Fedorov, I V Kulbakin, A V Vorobiev *Electrochem. Commun.* **20** 60 (2012)
129. V V Belousov, V A Schelkunov, S V Fedorov, I V Kulbakin, A V Vorobiev *Ionics* **18** 787 (2012)
130. RF P. 2400293 (2010)
131. V V Belousov *Zh. Fiz. Khim.* **81** 521 (2007) [g]
132. S V Fedorov, V V Belousov *Elektrokhimiya* **45** 609 (2009) [f]
133. V V Belousov *J. Eur. Ceram. Soc.,* **27** 3459 (2007)
134. E A Pastukhov, V I Musikhin, N A Vatolin *Elektricheskie Svoistva Nestekhiometricheskikh Oksidnykh Rasplavov* (Electric Properties of Nonstoichiometric Oxide Melts) (Moscow: Nauka, 1984)
135. V M Denisov, N V Belousova, S A Istomin, S G Bakhvalov, E A Pastukhov *Stroenie i Svoistva Rasplavlennykh Oksidov* (Structure and Properties of Molten Oxides) (Ekaterinburg: Institute of Metallurgy, Ural Branch of the Russian Academy of Sciences, 1999)

[a] — *Protect. Met. Phys. Chem. Surf. (Engl. Transl.)*
[b] — *Inorg. Mater. Appl. Res. (Engl. Transl.)*
[c] — *Russ. J. Inorg. Chem. (Engl. Transl.)*
[d] — *Inorg. Mater. (Engl. Transl.)*
[e] — *Colloid. J. (Engl. Transl.)*
[f] — *Russ. J. Electrochem. (Engl. Transl.)*
[g] — *Russ. J. Phys. Chem., Ser. A (Engl. Transl.)*